Int. J. Heat Mass Transfer. Vol. 27, No. 6, pp. 883–891, 1984
Printed in Great Britain

0017–9310/84 $3.00 + 0.00
Pergamon Press Ltd.

PREDICTION OF CRITICAL HEAT FLUX FOR ANNULAR FLOW IN TUBES TAKING INTO ACCOUNT THE CRITICAL LIQUID FILM THICKNESS CONCEPT

Y. KATTO

Department of Mechanical Engineering, University of Tokyo,
Hongo, Bunkyo-ku, Tokyo, Japan

(*Received* 13 *May* 1983)

Abstract—In the particular part of the annular flow regime that is encountered in the experiment of critical heat flux (CHF) made with short tubes, the prediction of CHF based on the annular flow hydrodynamic model exhibits a quite different character from that of experimental data. However, if the concept of the critical liquid film thickness, which has recently been proposed as the governing factor of the CHF in external flow-type saturated boiling, is introduced to the hydrodynamic model, CHF can be predicted well through the whole range of the annular flow regime. This fact is shown quantitatively in this paper employing the Levy annular flow hydrodynamic model. Verification has been made for water at 0.84, 2.95, 6.9, and 13.7 MPa, but since it gives nearly the same results for each pressure, only the results obtained for 6.9 MPa are illustrated.

NOMENCLATURE

- C concentration of liquid droplets in vapor core flow [kg m^{-3}]
- C_{eq} concentration in hydrodynamic equilibrium state [kg m^{-3}]
- d tube diameter [m]
- D deposition rate of droplets [kg m^{-2} s^{-1}]
- E entrainment rate of droplets [kg m^{-2} s^{-1}]
- f_{ig} friction factor
- G mass velocity, $W/(\pi d^2/4)$ [kg m^{-2} s^{-1}]
- G_{lF} liquid film mass velocity, $W_{lF}/(\pi d^2/4)$ [kg m^{-2} s^{-1}]
- H_{fg} latent heat of evaporation [J kg^{-1}]
- ΔH_i inlet subcooling enthalpy [J kg^{-1}]
- k_d deposition mass transfer coefficient [m s^{-1}]
- l heated tube length [m]
- p pressure [MPa]
- q heat flux [W m^{-2}]
- q_c critical heat flux [W m^{-2}]
- q_{co} critical heat flux for the case of $\Delta H_i = 0$ [W m^{-2}]
- W total mass flow rate [kg s^{-1}]
- W_{lF} mass flow rate of liquid film [kg s^{-1}]
- y_F thickness of liquid film [m]
- y_{F1} thickness of liquid film at $z = z_1$ [m]
- z axial distance ($\Delta H_i = 0$ at $z = 0$) [m]
- z_1 position at the start of annular flow [m].

Greek symbols

- α_1 void fraction at $z = z_1$
- β, β' entrainment parameters
- δ_c critical liquid film thickness [m]
- μ_l viscosity of liquid [Pa s]
- ρ_v density of liquid [kg m^{-3}]
- ρ density of vapor [kg m^{-3}]
- σ surface tension [N m^{-1}]
- τ_w wall shear stress [N m^{-2}]
- χ vapor quality
- χ_1 vapor quality at $z = z_1$
- χ_{eq} vapor quality in hydrodynamic equilibrium state
- χ_{ex} exit quality in CHF condition.

1. INTRODUCTION

THIS paper deals with the critical heat flux (CHF) of forced flow in uniformly heated vertical tubes excluding the extremely high pressure state. For this case, it is known that experimental data of the critical heat flux q_c obtained by changing the tube length l as well as the inlet subcooling enthalpy ΔH_i under a fixed condition of pressure p, tube diameter d, and mass velocity G, can be correlated, in the approximate sense, as a function of the exit quality χ_{ex}, which is determined via the heat balance as

$$\chi_{ex} = \frac{4q_c}{GH_{fg}}\frac{l}{d} - \frac{\Delta H_i}{H_{fg}}. \quad (1)$$

For the general character of the above-mentioned function $q_c = f(\chi_{ex})$, there are two concepts of a somewhat different nature as shown in Fig. 1.

Figure 1(a) represents the flux/quality curve postulated by Bennett *et al.* [1] with four characteristic regions on it. It is seen that the slope of the curve is gentle in regions I and III, but is steep in the intermediate region II, where quality hardly changes as against the change of heat flux. According to Hewitt [2], regions I–III are associated with the CHF in the annular flow regime, while the remaining region, region IV, is related to the CHF in the near-wall bubble crowding situation. To give a little more detail, the CHF in region I occurs mainly through the balance between droplet deposition and liquid film evaporation; then in region II, the flow of liquid from the upstream film also participates in determining CHF; and finally in region III, a large amount of entrainment exists at the onset of annular flow exerting a strong influence on CHF.

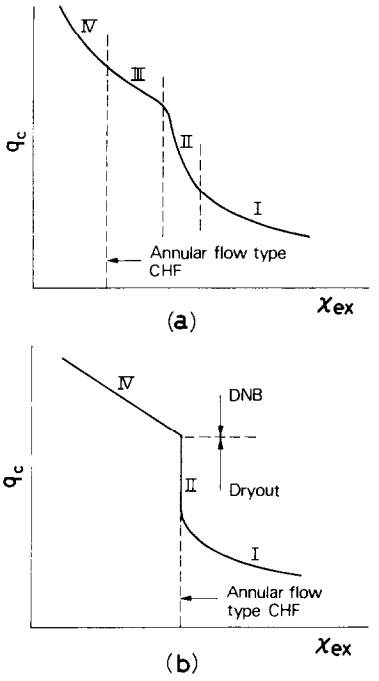

FIG. 1. Curve of critical heat flux as a function of exit quality for uniformly heated tubes with variable l and ΔH_i under a fixed condition of p, d and G.

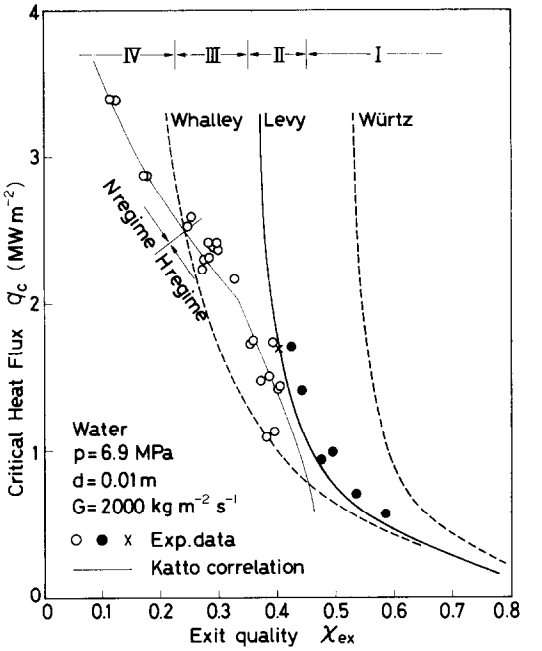

FIG. 2. Critical heat flux vs exit quality for the case of $\Delta H_i > 0$. Experimental data: ○, from Thompson and Macbeth (p = 6.7–7.1 MPa, d = 0.0108 m, l = 0.43–3.05 m, G = 1940–2090 kg m^{-2} s^{-1}); ●, from Würtz (p = 7.0 MPa, d = 0.01 m, l = 2.02–8.00 m, G = 2000 kg m^{-2} s^{-1}); and ×, from Milan reproducibility test data (p = 7.0 MPa, ΔH_i = 75 kJ kg^{-1}, d = 0.01 m, l = 2.00 m, G = 2000 kg m^{-2} s^{-1}).

The existing data with subcooled inlet conditions ($\Delta H_i > 0$) for water at p = 6.9 MPa, d = 0.01 m and G = 2000 kg m^{-2} s^{-1}, collected from Thompson and Macbeth [3], Würtz [4], and Milan reproducibility test data [5], are represented in Fig. 2. Note that these data points exhibit nearly the same trend as the curve in Fig. 1(a), permitting a rough classification of regions I–IV in such a way as shown by the directional lines at the top of Fig. 2. A thin curve near the data points in Fig. 2 represents the flux/quality curve* predicted by the present author's empirical generalized correlation: equations (A1)–(A4) in the Appendix, where the H regime corresponds to annular flow and the N regime to froth flow as has been shown in ref. [6]. Thus this is considered the same situation as in Fig. 1(a) with respect to the extent of the annular flow regime.

On the other hand, Fig. 1(b) is the flux/quality curve postulated by Doroschuk *et al.* [7] and other Soviet investigators [8], where regions I and II are said to be related to dryout-type CHF, while the remaining region IV to DNB-type CHF; and it is also said that in region I, CHF is dominated by droplet deposition, but in region II, droplet deposition is suppressed by a strong vapor effusion from the liquid film due to high heat fluxes, and thereby the exit quality χ_{ex} is kept constant.

Recently, France *et al.* [9] reported experimental results which were regarded as indirectly supporting the two-mechanism CHF in Fig. 1(b). Meanwhile, Levy *et al.* [10] attempted a computational calculation of CHF through their own annular flow hydrodynamic model giving the result shown by a thick line in Fig. 2, and discussed the relation to the particular part of region II of the CHF curve in Fig. 1(b).

It is well known that the CHF curve of regions I and II in Fig. 1(b) results from the data of the experiments made with the two-phase mixed inlet condition.† Accordingly the curve of Fig. 1(b) cannot be compared directly with that of Fig. 1(a). However, it seems justifiable to assume the respective correspondences of regions I, II and IV between Figs. 1(a) and (b), because of the similarities in the slope of the curve and the presumed CHF mechanism. And if so, it raises an important question of whether or not the annular flow-type CHF can be assumed in region III in Fig. 1(a) or Fig. 2. Because, if viewed from the standpoint of Fig. 1(b), DNB-type CHF should be assumed there.

Recently, Whalley *et al.* [14, 15], Würtz [4], Levy *et al.* [10], Saito *et al.* [16], Leung *et al.* [17], and others have performed interesting studies showing the reliability of the computational analysis of the annular flow-type CHF in channels based on their respective annular flow hydrodynamic models. However, it seems

* This curve shows a deviation from the data points in the range of $\chi_{ex} > 0.46$, which corresponds approximately to the condition of $l/d > 600$. See ref. [11] for the details of this problem.

† Recently Kitto [12] stated the possibility of obtaining the CHF curve of Fig. 1(b) even at the subcooled inlet condition, but as mentioned in ref. [13], it would seem that there is little reliable evidence for this.

likely that the above-mentioned problem has so far been left outside of the scope of study.

Incidentally, Haramura and Katto [18, 19] have recently succeeded in clarifying the CHF mechanism in external flow-type saturated boiling by means of the critical thickness δ_c of a liquid film stabilizing on a solid wall heated with a heat flux q, which is given in a generalized form as

$$\frac{\delta_c \rho_v}{\sigma}\left(\frac{q}{\rho_v H_{fg}}\right)^2 = \frac{\pi(0.0584)^2}{2}\left(1+\frac{\rho_v}{\rho_l}\right)\left(\frac{\rho_v}{\rho_l}\right)^{0.4}. \quad (2)$$

This equation indicates a rapid reduction of δ_c with increasing q, so that the thickness of the liquid film accompanying the annular flow in a tube may possibly be affected by δ_c when the heat flux is very high.

This paper reports the results of a study made to clarify the mechanism of the CHF in region III of Fig. 1(a) by introducing the concept of the critical film thickness into the annular flow hydrodynamic model.

2. CALCULATION OF CHF BY THE ANNULAR FLOW HYDRODYNAMIC MODEL

For the sake of simplicity, a uniformly heated vertical tube fed with a saturated liquid at the tube inlet will be considered from now on. In this case, annular flow starts at a location $z = z_1$ downstream of the tube inlet as shown in Fig. 3, and the mass balance equation of the liquid film for $z > z_1$ is written as

$$\frac{dG_{lF}}{dz} = \frac{4}{d}\left(D - E - \frac{q_{co}}{H_{fg}}\right), \quad (3)$$

where G_{lF} is the liquid film mass velocity, D the deposition rate, E the entrainment rate, and q_{co}/H_{fg} the evaporation rate (mass rate per unit area of the tube wall, respectively). If the deposition mass transfer coefficient k_d is introduced, $D = k_d C$ and $E = k_d C_{eq}$, where C is the liquid mass entrained per unit volume of the core vapor flow, and C_{eq} is the value of C in the hydrodynamic equilibrium state. In addition, the quality χ at an arbitrary location z is given via the heat balance as

$$\chi = \frac{4q_{co}}{GH_{fg}}\frac{z}{d}. \quad (4)$$

Thus employing the foregoing k_d and χ, equation (3) is rewritten as

$$\left.\begin{aligned} &\frac{d(G_{lF}/G)}{d\chi} = \Phi - 1, \\ &\text{where} \\ &\Phi = \frac{k_d \rho_l / G}{q_{co}/GH_{fg}}\left(\frac{C}{\rho_l} - \frac{C_{eq}}{\rho_l}\right). \end{aligned}\right\} \quad (5)$$

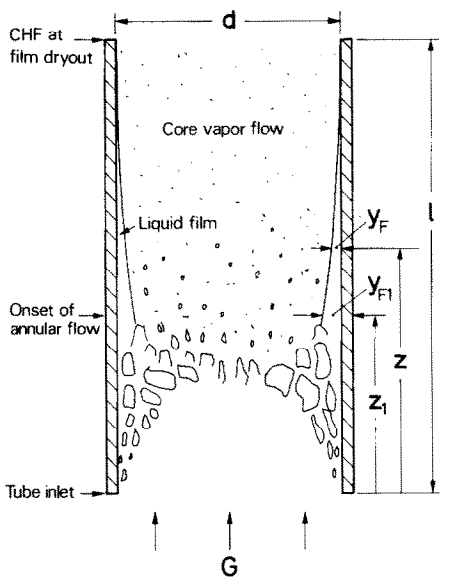

FIG. 3. Critical heat flux and liquid film behavior in an annular flow.

2.1. *Annular flow hydrodynamic model*

Proper estimates of k_d and C_{eq} are needed to execute the numerical integration of equation (5) on the computer. However, somewhat different procedures have so far been adopted in the respective existing studies particularly for the estimate of C_{eq}, and besides the conditions to specify the onset of annular flow are not necessarily identical. Therefore, three different models of Whalley *et al.* [14], Würtz [4], and Levy *et al.* [10] are chosen to be compared in Fig. 2, where the conditions adopted in the present calculation for each model are listed in Table 1.

It is seen in Fig. 2 that any of the models can predict the same trend as the experimental data points in regions I and II, qualitatively at least. However, the

Table 1. Conditions adopted to make the calculation of CHF for Fig. 2

Calculation model	Deposition k_d (m s^{-1})	Entrainment C_{eq} (kg m^{-3})	Entrainment E (kg m^{-2} s^{-1})	Onset of annular flow χ_1	Onset of annular flow α_1	Onset of annular flow State
Whalley *et al.*	0.01	Empirical value [1]	—	0.01	—	$C = C_{eq}$*
Würtz	0.01	—	Empirical formula [3]	—	0.8	$C = E/k_d$
Levy *et al.*	0.01	Semi-theoretical prediction [4]	—	—	0.8	$C = C_{eq}$

* Originally the condition of $G_{lF}/G = 0.01(1-\chi_1)$ was used instead of $C = C_{eq}$ by Whalley *et al.* [1]. The merit of the latter condition has been discussed in ref. [6].

Levy model employing the semi-theoretical evaluation method of C_{eq} developed by Levy and Healzer [20] is the best one for the quantitative agreement with the data. In addition, this model is based on the three-zone velocity distribution in a turbulent liquid film. In this paper, therefore, the Levy model will be employed below, then the local values of C/ρ_l and C_{eq}/ρ_l in equation (5) are evaluated by the following dimensionless equations, respectively

$$\frac{C}{\rho_l} = \frac{\rho_v}{\rho_l}\Big/\left\{\frac{\chi}{1-\chi-(G_{lF}/G)} - \frac{\rho_v}{\rho_l}\right\}, \tag{6}$$

$$\frac{C_{eq}}{\rho_l} = \frac{\rho_v}{\rho_l}\Big/\left\{\frac{\chi_{eq}}{1-\chi_{eq}-(G_{lF}/G)} - \frac{\rho_v}{\rho_l}\right\}, \tag{7}$$

where χ_{eq} in equation (7) is given as the root of equations (8)–(10)

$$\left.\begin{aligned} \chi_{eq} &= 1 - \frac{G_{lF}/G}{1-\sqrt{(1/\beta)}} \quad \text{for } y_F^+ \geqslant 30, \\ \chi_{eq} &= 1 - \frac{G_{lF}/G}{1-\sqrt{(1/\beta')}} \quad \text{for } y_F^+ < 30, \end{aligned}\right\} \tag{8}$$

where β, designated as the entrainment parameter, is the root of

$$\beta = 1 + \sqrt{\left\{\frac{2}{0.4\chi_{eq}^2}\frac{\sigma\rho_l}{G^2 d}\left[\left(\frac{\rho_l}{\rho_v}\right)^{1/\beta} - 1\right]\right\}},$$

and β' is given by

$$\beta' = 1 + \sqrt{2(\beta - 1)}.$$

The dimensionless film thickness y_F^+ included in equation (8) is related to the film mass velocity G_{lF} as well as the wall shear stress τ_w as

$$\frac{G_{lF}}{G}\frac{G/\rho_l}{\sqrt{(\tau_w/\rho_l)}} = \frac{2}{r_o^{+2}} K(y_F^+, r_o^+), \tag{9}$$

where r_o^+, y_F^+ and $K(y_F^+, r_o^+)$ are

$$r_o^+ = \frac{(d/2)\sqrt{(\tau_w/\rho_l)}}{\mu_l/\rho_l}, \quad y_F^+ = \frac{y_F\sqrt{(\tau_w/\rho_l)}}{\mu_l/\rho_l},$$

and

$$K(y_F^+, r_o^+) = r_o^+ y_F^{+2}/2 + y_F^{+3}/3 \quad \text{for } y_F^+ < 5,$$

$$K(y_F^+, r_o^+) = 12.51 r_o^+ - 10.45 - 8.05 r_o^+ y_F^+ + 2.775 y_F^{+2} + 5 r_o^+ y_F^+ - 2.5 y_F^+ \ln y_F^+ \quad \text{for } 5 < y_F^+ < 30,$$

$$K(y_F^+, r_o^+) = 3 r_o^+ y_F^+ - 63.9 r_o^+ - 2.125 y_F^{+2} - 1.25 y_F^{+2} \ln y_F^+ + 2.5 r_o^+ y_F^+ \ln y_F^+ + 573.21 \quad \text{for } 30 < y_F^+.$$

The foregoing shear stress τ_w is evaluated through the Wallis equation [21] as

$$\tau_w = f_{ig}\frac{1}{2}\rho_v\left(\frac{G\chi_{eq}}{\rho_v}\right)^2, \tag{10}$$

where f_{ig} is the friction factor given as a function of y_F as

$$f_{ig} = 0.005\left(1 + 300\frac{y_F}{d}\right).$$

2.2. *Deposition coefficient k_d and initial conditions*

As for the deposition coefficient k_d on the RHS of equation (5), no generalized correlation has been given yet, but the empirical values prepared by Whalley *et al.* [14] are available for water at pressures ranging from 0.2 to 18 MPa. For the sake of simplicity, they are correlated in this paper as

$$\left.\begin{aligned} k_d\,[\text{m s}^{-1}] &= 0.405\sigma^{0.915} \quad \text{for } \sigma < 0.0383 \text{ N m}^{-1}, \\ k_d\,[\text{m s}^{-1}] &= 9.48\times 10^4\sigma^{4.70} \quad \text{for } \sigma > 0.0383 \text{ N m}^{-1}. \end{aligned}\right\} \tag{11}$$

Next, the axial position where the annular flow pattern starts (see Fig. 3) is specified by a designated value of the void fraction α_1 as well as by the condition of $C = C_{eq}$, or $\chi = \chi_{eq}$ from equations (6) and (7). The former condition determines the initial liquid film thickness y_{F1} as

$$y_{F1}/d = (1 - \sqrt{\alpha_1})/2, \tag{12}$$

and the latter condition cooperates with equations (8)–(10) to determine the initial values of χ_{eq}, G_{lF}/G and $\chi\,(=\chi_1)$, respectively, corresponding to the magnitude of y_{F1} given by equation (12).

2.3. *Prediction of CHF*

According to equation (1), χ_{ex} is a value determined under the influence of q_c, suggesting that χ_{ex} is not considered as an independent variable toward q_c. In addition, it is known that q_c is not a unique function of χ_{ex} in the strict sense of the word. Thus the correlation of data in the form of Fig. 2 is not necessarily suitable for the study of the CHF mechanism.

Then the boiling length, that is the axial distance from the position of $\chi = 0$ to the tube exit end, is determined for each data point in Fig. 2, and if it is taken as a tube length l, then $\Delta H_i = 0$ holds for this tube, so q_c can be rewritten as q_{co} resulting in the alternative correlation of data in the form of Fig. 4.

Meanwhile, thick solid lines in Fig. 4 represent the prediction of CHF given by equations (4)–(12) for initial void ratios of $\alpha_1 = 0.1$, 0.6, 0.8, 0.9, and 0.95, respectively, where $\alpha_1 = 0.1$, 0.9, and 0.95 have been shown only for information because they are either too small or too large as the void fraction to specify the onset of annular flow. It can be noted that the predictions in the region of $l/d > 200$ are insensitive to the value of α_1, and at the same time, agree well with the experimental data, while those in the region of $l/d < 200$ show dispersion due to α_1 as well as disagreement with the trend of the experimental data.

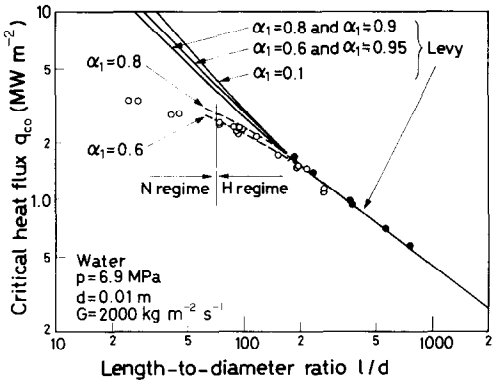

FIG. 4. Critical heat flux vs length-to-diameter ratio for the case of $\Delta H_i = 0$ with the same data symbols as those in Fig. 2.

3. INTRODUCTION OF CRITICAL LIQUID FILM THICKNESS CONCEPT

3.1. *Initial liquid film thickness* y_{F1}

The results of Fig. 4 show the following interesting facts. First, the Levy model is successful in predicting CHF when it is not affected by the initial void fraction α_1, suggesting the reliability of the model except for the function of the initial conditions. Second, the Levy model employing the initial conditions based on equation (12) is unsuccessful with comparatively short tubes for any value of α_1 from 0.1 to 0.95, showing that equation (12) is unsuitable to determine the initial liquid film thickness y_{F1} in the range of $l/d \doteqdot 70 \sim 200$ in Fig. 4.

Now the alternative to equation (12) must be found, and it is not a difficult task because there is a restriction of equation (2) on the thickness of a liquid film stabilizing on a heated wall, which means that equation (12) is invalid when the heat flux is so high that δ_c from equation (2) is less than y_{F1} from equation (12), that is

$$\delta_c/d < (1-\sqrt{\alpha_1})/2. \tag{13}$$

Under this condition, the initial film thickness y_{F1} must be determined by equating it to the δ_c from equation (2) as

$$\frac{y_{F1}}{d} = \frac{\delta_c}{d} = \frac{\pi(0.0584)^2}{2} \times \frac{\sigma\rho_l/G^2 d}{(q_{co}/GH_{fg})}\left(1+\frac{\rho_v}{\rho_l}\right)\left(\frac{\rho_v}{\rho_l}\right)^{1.4}. \tag{14}$$

3.2. *Initial quality* χ_1

When the film thickness y_{F1} at the starting location of annular flow is given by equation (14) instead of equation (12), the flow configuration near this location must be different from that assumed in the annular flow hydrodynamic model. However, according to the data points in Fig. 4, the magnitude of q_{co} changes by only about 1.5 times within the range of $l/d \doteqdot 70 \sim 200$, then y_{F1} of equation (14) does not reduce to less than, say, half the value of y_{F1} given by equation (12). In addition, the magnitude of y_{F1}/d of equation (12) itself is essentially small ($y_{F1}/d = 0.133$–0.053 for $\alpha_1 = 0.6$–0.8). Therefore, it can be assumed approximately that the flow configuration near the starting location of annular flow is still dominated rather strongly by the annular flow hydrodynamics.

Thus, in the analysis below, the initial film thickness y_{F1} will be determined by equation (14) when inequality (13) holds, while by equation (12) when inequality (13) does not hold. As for the initial quality χ_1, however, it will be determined by the method of Section 2.2 independent of the condition of inequality (13) for the sake of simplicity.

3.3. *Dominant role of evaporation in high heat flux region*

Under given conditions of p, d and G, if the critical heat flux q_{co} is sufficiently high, Φ can be neglected on the RHS of equation (5). A numerical example is shown in Fig. 5, where solid lines are the same as those in Fig. 4, and broken lines are the Levy model predictions of q_{co} obtained through equation (4) in the ideal case of putting $\Phi = 0$ in equation (5). Note that except for the absurd case of $\alpha_1 = 0.1$, the behavior of the liquid film flow is practically controlled by the evaporation of the film in the high heat flux region, causing the dispersion of the prediction due to the initial void fraction α_1 as well.

Exactly speaking, the configuration of the annular flow along the tube involving the condition of inequality (13) must differ from that assumed in the annular flow hydrodynamic model. However, the foregoing results of Fig. 5 suggest that in the high heat flux region under consideration, the reduction of the liquid film thickness in the direction of flow is caused mainly by the evaporation from the film regardless of the flow configuration. Therefore, in the present analysis, Φ in equation (5) will be assumed to be

$$\Phi = 0, \tag{15}$$

when inequality (13) holds.

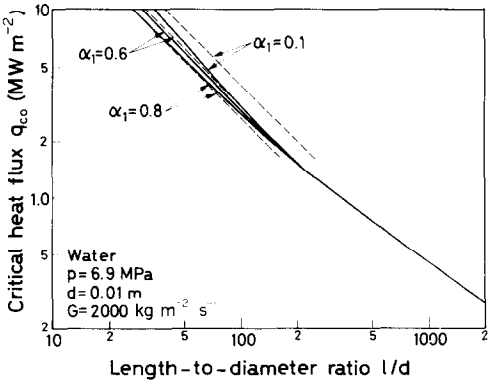

FIG. 5. Comparison between Levy model predictions and those obtained in the ideal case assuming a pure evaporation mechanism of liquid film.

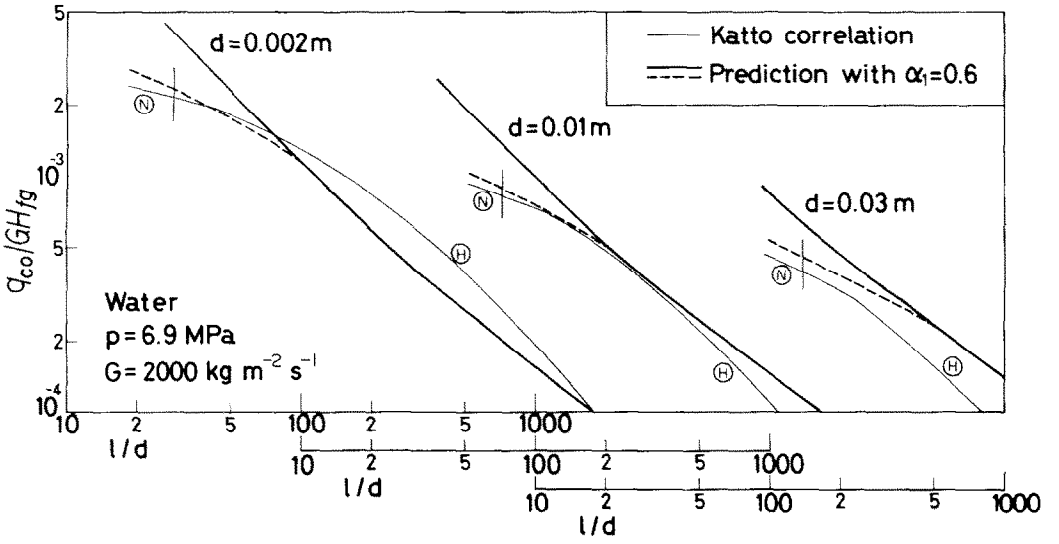

FIG. 6. Comparison between the predicted and the experimental CHF for the case of $G = 2000\ \text{kg m}^{-2}\ \text{s}^{-1}$.

3.4. *Comparison between predicted and experimental CHF*

The Levy model modified in Sections 3.1–3.3 gives the CHF predictions shown by broken lines in Fig. 4 for $\alpha_1 = 0.6$ and 0.8, showing fairly good agreement with the experimental data. It is difficult to answer the question of which value of α_1 is more correct from the physical point of view, because a few approximations such as those mentioned in Sections 3.2 and 3.3 have been adopted in predicting CHF. However, for the agreement with the data points in Fig. 4, $\alpha_1 = 0.6$ is superior to $\alpha_1 = 0.8$, accordingly it will be assumed below that constantly

$$\alpha_1 = 0.6. \tag{16}$$

Then the computational predictions of CHF for various conditions are compared with the experimental results in Fig. 6 for the case of $G = 2000\ \text{kg m}^{-2}\ \text{s}^{-1}$, Fig. 7 for the case of $G = 100\ \text{kg m}^{-2}\ \text{s}^{-1}$, and Fig. 8 for the case of variable G. Since it is impossible to collect the systematic data for each prescribed condition, the present author's generalized correlation of equations (A1)–(A3) in the Appendix, which agree fairly well with the experimental data as shown in ref. [22], are employed as a substitute giving thin lines marked (L), (H) and (N) in Figs. 6–8. Short vertical lines in these three figures represent the boundary between N and H regimes predicted by equation (A4), indicating the annular flow regime on the RHS of each line.

In Figs. 6–8, thick solid lines show the computational

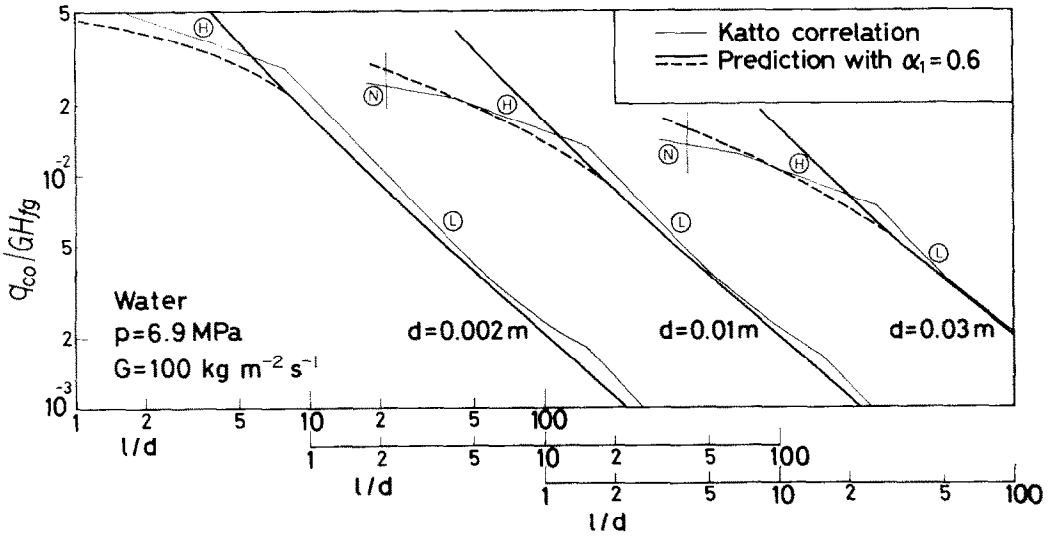

FIG. 7. Comparison between the predicted and the experimental CHF for the case of $G = 100\ \text{kg m}^{-2}\ \text{s}^{-1}$.

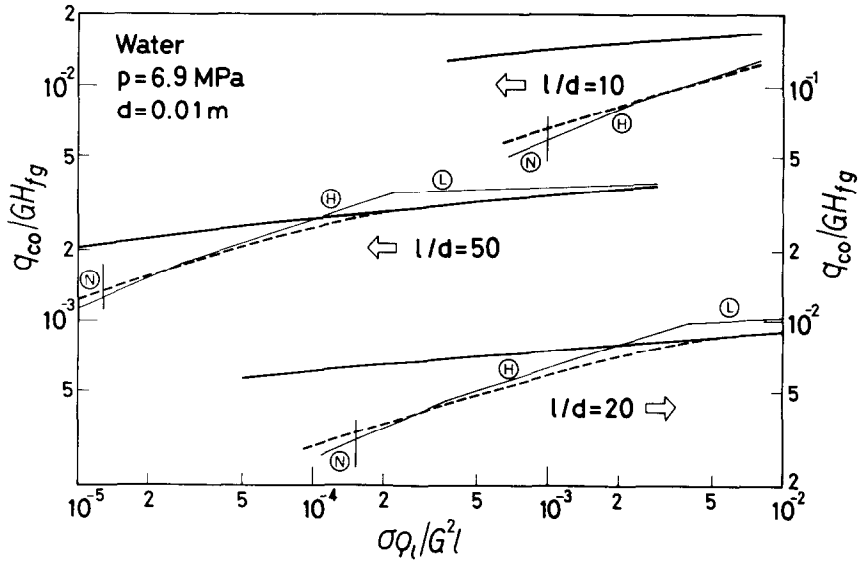

FIG. 8. Comparison between the predicted and the experimental CHF for the case of variable G.

predictions made through the Levy hydrodynamic model of equations (4)–(12), while broken lines represent the predictions obtained by the Levy model modified with the critical liquid film thickness concept of equations (13) and (14) and the supplementary conditions mentioned in Sections 3.2 and 3.3. Note that broken lines agree well with the experimental trend in the part of the annular flow regime where thick solid lines fail to follow the experimental trend. It is added here that similar results have been obtained for $p = 0.84$, 2.95 and 13.7 MPa as well, though the presentation is omitted in this paper to save space.

4. CONCLUSIONS

(1) The Levy annular flow hydrodynamic model is quite successful in predicting CHF for comparatively long tubes, but fails to explain the special trend of experimental data in the part of the annular flow regime encountered in the experiments made with comparatively short tubes and accordingly with high values of CHF.

(2) The serious fault mentioned above is removed by modifying the Levy model so as to determine the initial film thickness by equation (14) instead of equation (12) when inequality (13) holds. The CHF predictions thus obtained are satisfactorily compared with the experimental data of water covering a wide range of test pressures.

(3) The fluid configuration postulated in the foregoing modified Levy model is in accord with Hewitt's view mentioned in the Introduction that region III in Fig. 1(a) is characterized by a large amount of entrainment at the onset of annular flow, because the reduction of the initial film thickness is accompanied by the increase of the entrainment at the onset of annular flow.

(4) According to the results of the present study, it seems incorrect to assume the DNB-type mechanism throughout region IV of Fig. 1(b).

(5) The present study shows that there is a natural connection of the CHF mechanism between the external flow-type saturated boiling and the flow boiling in comparatively short tubes with subcooled inlet conditions.

Acknowledgement—The support for this work provided by the Ministry of Education, Science and Culture: Special Project Research on Energy, Grant No. 58040020 (1983) is gratefully acknowledged.

REFERENCES

1. A. W. Bennett, G. F. Hewitt, H. A. Kearsey, R. K. F. Keeys and D. J. Pulling, Studies of burnout in boiling heat transfer, *Trans. Instn Chem. Engrs* **45**, T319–T339 (1967).
2. G. F. Hewitt, Burnout, in *Handbook of Multiphase Systems* (edited by G. Hetsroni), pp. 6.66–6.141. Hemisphere, Washington, DC (1982).
3. B. Thompson and R. V. Macbeth, Boiling water heat transfer burnout in uniformly heated round tubes: a compilation of world data with accurate correlations, UKAEA, AEEW-R 356 (1964).
4. J. Würtz, An experimental and theoretical investigation of annular steam–water flow in tubes and annuli at 30 to 90 bar, Risø National Laboratory, Denmark, Risø Report No. 372 (1978).
5. K. M. Becker, J. Bager and D. Djursing, Burnout correlations in simple geometries: most recent assessments, in *Seminar on Two-phase Flow Thermohydraulics*, Rome, pp. 51–91 (1972).
6. Y. Katto, An analytical investigation on CHF of flow boiling in uniformly heated vertical tubes with special reference to governing dimensionless groups, *Int. J. Heat Mass Transfer* **25**, 1353–1361 (1982).
7. V. E. Doroschuk, L. L. Levitan and F. P. Lantzman, Investigations into burnout in uniformly heated tubes, ASME-Paper 75-WA/HT-22 (1975).
8. Scientific Council, U.S.S.R. Academy of Sciences, Recommendation on calculating burnout when boiling

water in uniformly heated round tubes, BTD OKB IVTAN, Moscow (1975).
9. D. M. France, T. Chiang, R. D. Carlson and R. Priemer, Experimental evidence supporting two-mechanism critical heat flux, *Int. J. Heat Mass Transfer* **25,** 691–698 (1982).
10. S. Levy, J. M. Healzer and D. Abdollahian, Prediction of critical heat flux for annular flow in vertical pipes, EPRI NP-1619 (1980).
11. Y. Katto, A study on limiting exit quality of CHF of forced convection boiling in uniformly heated vertical channels, *Trans. Am. Soc. Mech. Engrs*, Series C, *J. Heat Transfer* **104,** 40–47 (1982).
12. J. B. Kitto, Jr., Critical heat flux and the limiting quality phenomenon, *A.I.Ch.E. Symp. Ser.* **76**(199), 57–78 (1980).
13. Y. Katto, Critical heat flux in forced convective flow, in *ASME JSME Thermal Engineering Joint Conference Proceedings*, Vol. 3, pp. 1–10 (1983).
14. P. B. Whalley, P. Hutchinson and G. H. Hewitt, The calculation of critical heat flux in forced convection boiling, in *Proc. 5th Int. Heat Transfer Conf.*, Tokyo, Vol. IV, pp. 290–294 (1974).
15. P. B. Whalley, P. Hutchinson and P. W. James, The calculation of critical heat flux in complex situations using an annular flow model, in *Proc. 6th Int. Heat Transfer Conf.*, Toronto, Vol. 5, pp. 65–70 (1978).
16. T. Saito, E. D. Hughes and M. W. Carbon, Multi-fluid modeling of annular two-phase flow, *Nucl. Engng Des.* **50,** 225–271 (1978).
17. A. Leung, S. Banerjee and D. C. Groeneveld, Investigation of the effects of heater characteristics on CHF performance of a long vertical annuli in high pressure water, in *Proc. 7th Int. Heat Transfer Conf.*, Munich, Vol. 4, pp. 303–308 (1982).
18. Y. Haramura and Y. Katto, A new hydrodynamic model of critical heat flux, applicable widely to both pool and forced convection boiling on submerged bodies in saturated liquids, *Int. J. Heat Mass Transfer* **26,** 389–399 (1983).
19. Y. Katto and Y. Haramura, Critical heat flux on a uniformly heated horizontal cylinder in an upward cross flow of saturated liquid, *Int. J. Heat Mass Transfer* **26,** 1199–1205 (1983).
20. S. Levy and J. M. Healzer, Application of mixing length theory to wavy turbulent liquid–gas interface, *Trans. Am. Soc. Mech. Engrs*, Series C, *J. Heat Transfer* **103,** 492–500 (1981).
21. G. B. Wallis, Annular two-phase flow, Part 1: a simple theory, *Trans. Am. Soc. Mech. Engrs*, Series D, *J. Basic Engng* **92,** 59–72 (1970).
22. Y. Katto, General features of CHF of forced convection boiling in uniformly heated vertical tube with zero inlet subcooling, *Int. J. Heat Mass Transfer* **23,** 493–504 (1980).
23. Y. Katto, Critical heat flux of forced convection boiling in uniformly heated vertical tubes (correlation of CHF in HP-regime and determination of CHF-regime map), *Int. J. Heat Mass Transfer* **23,** 1573–1580 (1980).

APPENDIX

From the correlation equations derived by the present author [23] for round tubes, only those necessary in this paper are shown below. The lowest value among those of q_{co} evaluated from equations (A1) to (A3) gives the critical heat flux q_{co} for a given condition. Note that equations (A2) and (A3) are unapplicable to the range of $l/d > 600$ (cf. ref. [11]).

L regime:

$$\frac{q_{co}}{GH_{fg}} = C\left(\frac{\sigma\rho_l}{G^2 l}\right)^{0.043}\frac{1}{l/d}, \tag{A1}$$

where $C = 0.25$ for $l/d < 50$, $C = 0.34$ for $l/d > 150$, and $C = 0.25 + 0.0009\{(l/d) - 50\}$ for $l/d = 50$–150.

H and N regime:

$$\frac{q_{co}}{GH_{fg}} = 0.1\left(\frac{\rho_v}{\rho_l}\right)^{0.133}\left(\frac{\sigma\rho_l}{G^2 l}\right)^{1/3}\frac{1}{1+0.0031\,l/d}, \tag{A2}$$

$$\frac{q_{co}}{GH_{fg}} = 0.098\left(\frac{\rho_v}{\rho_l}\right)^{0.133}\left(\frac{\sigma\rho_l}{G^2 l}\right)^{0.433}\frac{(l/d)^{0.27}}{1+0.0031\,l/d}, \tag{A3}$$

where the boundary between H and N regime is given by

$$\frac{l}{d} = \frac{0.77}{(\sigma\rho_l/G^2 l)^{0.37}}. \tag{A4}$$

CALCUL DU FLUX CRITIQUE POUR L'ECOULEMENT ANNULAIRE DANS LES TUBES A PARTIR DU CONCEPT D'EPAISSEUR CRITIQUE DU FILM LIQUIDE

Résumé—Dans le cas particulier du régime d'écoulement annulaire rencontré dans les expériences de flux thermique critique (CHF) pour les tubes courts, le calcul de CHF basé sur le modèle hydrodynamique dénote un caractère très différent des données expérimentales. Néanmoins si le concept d'épaisseur critique du film liquide, qui a été récemment proposé comme le facteur déterminant de CHF dans l'ébullition saturée externe, est introduit dans le modèle hydrodynamique, le CHF peut être prédit correctement pour le domaine complet du régime annulaire. Ce fait est quantitativement traité dans cet article en employant le modèle hydrodynamique de Levy. Une vérification a été faite pour l'eau à 0,84, 2,95, 6,9 et 13,7 MPa, mais comme les résultats sont très proches pour toutes les pressions, seuls sont illustrés résultats obtenus pour 6,9 MPa.

BERECHNUNG DER KRITISCHEN WÄRMESTROMDICHTE BEI RINGSTRÖMUNG IM ROHR UNTER BERÜCKSICHTIGUNG DES KONZEPTS DER KRITISCHEN FLÜSSIGKEITSFILMDICKE

Zusammenfassung—In dem speziellen Teil des Ringströmungs-Gebiets, das im Experiment zur kritischen Wärmestromdichte (CHF) in kurzen Rohren auftritt, zeigt die Berechnung von CHF auf der Basis des hydrodynamischen Modells für die Ringströmung ein ganz anderes charakteristisches Verhalten als das der experimentellen Daten. Wenn jedoch das Konzept der kritischen Flüssigkeitsfilmdicke, das kürzlich als der maßgebliche Faktor für CHF bei äußerem strömungsartigen Sättigungssieden vorgeschlagen worden ist, in das hydrodynamische Modell eingeführt wird, kann CHF im gesamten Ringströmungs-Gebiet gut berechnet werden. Unter Verwendung des hydrodynamischen Modells von Levy für das Ringströmungs-Gebiet wird dies hier quantitativ gezeigt und für Wasser bei 0,84; 2,95; 6,9 und 13,7 MPa bestätigt. Da sich für jeden Druck nahezu die gleichen Resultate ergeben, werden nur die Ergebnisse für 6,9 MPa erläutert.

РАСЧЕТ КРИТИЧЕСКОГО ТЕПЛОВОГО ПОТОКА ПРИ КОЛЬЦЕВОМ ТЕЧЕНИИ В ТРУБАХ С УЧЕТОМ ПОНЯТИЯ КРИТИЧЕСКОЙ ТОЛЩИНЫ ПЛЕНКИ ЖИДКОСТИ

Аннотация—В частном случае кольуевого режима течения, который встречается в экспериментах по исследованию критического теплового потока (КТП) в коротких трубах, величина КТПа, рассчитываемая на основе гидродинамической модели кольцевого течения, сильно отличается от измеряемой экспериментально. Однако, если в гидродинамическую модель ввести понятие критической толщины пленки жидкости, предложенное недавно в качестве определяющего параметра КТПа для случая кипения насыщенной жидкости при течении, то величину КТПа можно адекватно рассчитать для всей области кольцевого режима течения. Для подтверждения приведены расчетные зависимости, полученные с помощью гидродинамической модели Леви для кольцевого течения. Расчеты проводились для воды при давлении 0,84; 2,95; 6,9 и 13,7 МПа, но так как результаты для всех случаев оказались почти одинаковыми, в статье представлены результаты только для давления 6,9 МПа.